applied sciences

MDPI

Communication

Fabrication of a New Air-Gap FBAR on an Organic Sacrificial Layer through an Innovative Design Algorithm

Giovanni Niro [1,2,*,†], Ilaria Marasco [1,2,†], Francesco Rizzi [2], Antonella D'Orazio [1], Marco Grande [1] and Massimo De Vittorio [2,3]

1 Dipartimento di Ingegneria Elettrica e dell'Informazione (DEI), Politecnico di Bari, Via Edoardo Orabona, 4, 70126 Bari, Italy
2 Center for Biomolecular Nanotechnology (CBN), Istituto Italiano di Tecnologia, Via Eugenio Barsanti, 14, 73010 Arnesano, Italy
3 Dipartimento di Ingegneria dell'Innovazione, Università del Salento, Via Lecce-Monteroni, 73047 Monteroni di Lecce, Italy
* Correspondence: giovanni.niro@poliba.it
† These authors equally contributed to this work.

Featured Application: Rapid prototyping of thin-film acoustic wave resonators with high precision.

Abstract: Realizing thin-film acoustic wave resonators presents many design and fabrication challenges. Actual material specifications always differ from nominal material properties employed in simulations, as they depend on the deposition technique and parameters used and on equipment type and status. Moreover, each deposition process introduces a degree of uncertainty regarding the thicknesses of the layers. All these factors have a substantial impact on the resonance frequency, which often differs from the designed value. This work details the design and fabrication of an aluminum nitride (AlN)-based thin-Film Bulk Acoustic wave Resonator (FBAR) showing one of the highest products of Q-factor and electromechanical coupling of 6895. The design process is based on an innovative, fast, and scalable design and fabrication approach that considers fabrication tolerances. The algorithm returns very fast results on the order of seconds, and successfully estimates the resonance of a designed stack at 2.55 GHz with a very low error of 0.005 GHz (about 0.2%). The FBAR layer stack is suspended on a polymeric membrane and an innovative rapid dissolving sacrificial layer made of Lift-Off Resist (LOR). This new fabrication protocol obtains resonators with an electromechanical coupling factor of 4.7% and a maximum quality factor of 1467, respectively.

Keywords: thin-film acoustic wave resonators; flexible resonators; Monte Carlo simulations; rapid-prototyping

Citation: Niro, G.; Marasco, I.; Rizzi, F.; D'Orazio, A.; Grande, M.; De Vittorio, M. Fabrication of a New Air-Gap FBAR on an Organic Sacrificial Layer through an Innovative Design Algorithm. *Appl. Sci.* **2023**, *13*, 1295. https://doi.org/10.3390/app13031295

Academic Editor: Edik U. Rafailov

Received: 21 November 2022
Revised: 11 January 2023
Accepted: 16 January 2023
Published: 18 January 2023

Copyright: © 2023 by the authors. Licensee MDPI, Basel, Switzerland. This article is an open access article distributed under the terms and conditions of the Creative Commons Attribution (CC BY) license (https://creativecommons.org/licenses/by/4.0/).

1. Introduction

Thin-Film Bulk Acoustic-wave Resonators (FBARs) represent one of the most promising technologies concerning other microelectromechanical resonators [1,2]. An FBAR consists of a stack formed of a piezoelectric layer sandwiched between two electrodes on a suspended cavity (back-trench and air-gap) or an acoustic Bragg grating (Surface-Mounted Resonators, SMR) [3,4]. The fabrication of the first FBAR was reported in 1980 [5], and nowadays, with the maturity of their fabrication processes [6], this technology has gained remarkable interest.

FBARs present unique features: they can easily reach frequencies between 1 and 20 GHz [7] and are characterized by the highest Q-factor and the smallest footprint reported in the literature [8] and a low insertion loss combined with high selectivity [9]. In addition, their fabrication process allows large-scale production as it is fully compatible with silicon-integrated circuit technology. All these features make them the world's smallest and best-performing resonator technology [10].

The commonly used simulation methods for the design of FBARs, such as the Equivalent Circuit Analysis (ECA) [11] and the Finite Element Method (FEM) [12–14], always require knowledge of the specifications of the materials composing the stack. These specifications can differ from the experimental ones, as they depend on the equipment technology and status, the deposition recipes, environmental conditions, and so on. Furthermore, each deposition process introduces a degree of uncertainty on the thickness of each layer due to the fabrication tolerances. The latter becomes a crucial challenge to overcome as even small variations in the top electrode thickness cause resonant frequency drift because of the mass-loading effect. Moreover, the design procedure loses validity if the piezoelectric thickness changes. All these drawbacks, if included in the commonly used models, increase the computational time [12].

In Reference [15], the FEM simulations were combined with a deep learning approach based on artificial neural networks; however, thousands of simulated data samples are necessary, making the method unsuitable for fast prototyping.

By contrast, in Reference [16], this problem was treated using FEM simulations whose parameters were refined with a closed feedback loop to minimize the error with measurements; however, this approach requires a very high computational cost as it exploits 3D FEM simulations.

In addition to the design problems, using a back trench to withstand the structure causes resonator fragility. The use of SMR structures prevents the release of the piezoelectric layer but lowers the performance compared to other solutions [8]. The trade-off between the two approaches is represented by air-gap types, where the structure is suspended on a thin membrane fabricated by employing a sacrificial process [6,17,18]. The presence of a membrane support layer ensures higher robustness, but also, in this case, the fragility of the suspended structure is an open issue in the case of FBARs working with very thin films [17]. Moreover, removing the sacrificial layer always requires aggressive chemicals that can damage the other materials, complicating their integration and increasing times and costs.

In this scenario, the fabrication of the first air-gap FBAR based on a highly soluble organic sacrificial layer made of Lift-Off Resist (LOR) and suspended on a polymeric flexible membrane is presented. Unlike other air-gap structures reported in the literature, with the innovative proposed fabrication protocol, the removal of the sacrificial material becomes very straightforward as it does not require any aggressive chemicals. In addition, in contrast to the state of the art, the presence of the flexible membrane support layer enhances the robustness of the structure by avoiding the formation of cracks and the collapse of the stack.

The resonator was developed by a new design approach based on an ad hoc proprietary algorithm and a proper material library comprising the most common metals used in the Microelectromechanical Systems (MEMS) industry. The advantage of this approach is the very low computational cost and the possibility to include both fabrication tolerances by means of Monte Carlo simulations and experimental material properties at the design level. Moreover, the modularity of the algorithm allows for including new materials using the systematic procedure detailed in the next sections without any modification of the code.

Finally, several experimental characterizations of both the design process and the fabrication protocol were reported to demonstrate the effectiveness of the algorithm. More in detail, the device was validated from a technological (by means of an optical microscope and a Scanning Electron Microscope, SEM, inspection) and an electronic point of view. The resonant frequency of the FBAR was correctly estimated by the design algorithm at 2.55 GHz with a very low error of 0.005 GHz (about 0.2%). The fabrication protocol was taken using a high-performance resonator having an electromechanical coupling factor of 4.7%, and very high quality factors of 1426 and 1477 for the resonance and antiresonance, respectively.

2. Materials and Methods

2.1. Design Algorithm

The design algorithm comprises three main building blocks: the decision core, the random perturbator, and the shared dataset.

The decision core takes the materials and the working frequency as inputs and returns the set of solutions. Each solution is characterized by a specific piezoelectric height allowing the user to select the best fabrication constraints and times. After choosing a single-stack solution, the random perturbator estimates the probability density function of the resonance value considering the fabrication tolerances of the deposition processes.

The decision core and the random perturbator are based on a material library. The central library can be easily expanded with new materials without any modifications to the algorithm using the systematic procedure detailed below.

2.2. Study for New Calibration Curves

The thicknesses of the piezoelectric material (d) and all the layers below it need to be set to obtain a calibration curve. Then, resonators with varying top electrode heights (h) are fabricated. The greater the mass of the top electrode, the lower the phase velocity (v_p). Therefore, variations in h translate into a resonant frequency drift (f_r).

The calibration curves are determined by fixing the piezoelectric thickness (d) and varying the top electrode (h). The value of f_r is evaluated for all h in the study, and then the corresponding phase velocities are obtained using Equation (1):

$$V_p = (2d)(f_r) \quad (1)$$

where d is the piezoelectric thickness and v_p is the acoustic phase velocity.

The corresponding value of the phase velocity is taken from Equation (1) for each resonator with different top electrode heights (h). Finally, the calibration curve of the phase velocity is expressed as a function of the ratio h/d.

The systematic study can be performed with FEM simulations or with experimental data. It is underlined that the reuse of past information is a crucial advantage of the proposed approach.

Figure 1 reports the calibration curves related to the commonest materials used in the MEMS industry (aluminum, titanium, copper, silver, molybdenum, and gold), obtained considering a 1 µm thick aluminum nitride piezoelectric layer and 160 nm thick molybdenum bottom electrode (see Figure 1a). The values of the calibration curves are derived using FEM parametric sweeps varying the metal and are reported in Figure 1b.

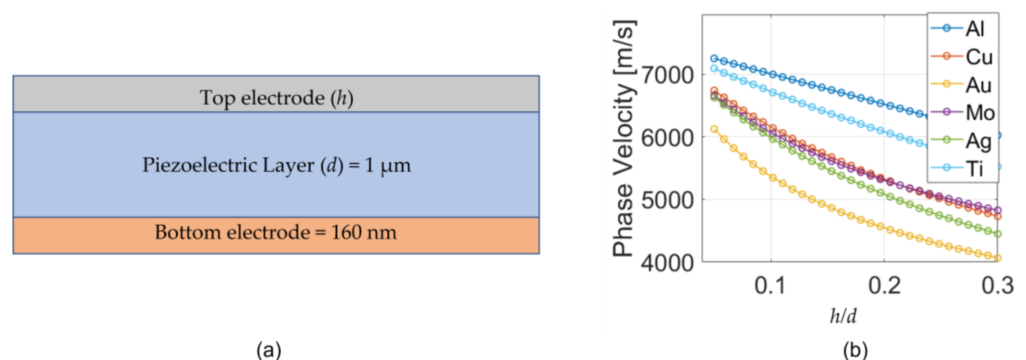

Figure 1. Material library of the design algorithm. (**a**) Cross-section of the model used for the systematic studies. (**b**) Obtained calibration curves.

2.3. Decision Core

The decision core is responsible for the design of the layers composing the stack starting from the specification of the resonance value and the materials. To simplify the

notation from here onward, we refer to the metal over piezoelectric thickness ratio (h/d) as k.

The solution provided by the decision core is a set of N resonators having different k-ratios but the same resonance frequency determined as in Equation (2):

$$A = \{k_1, k_2, \ldots, k_i, k_{(i+1)}, \ldots, k_N\} \quad (2)$$

The procedure starts from the materials specified by the user for guessing a set of possible phase velocities of the acoustic wave travelling back and forth in the resonating area (see Equation (3)):

$$V = \{v_{p1}, v_{p2}, \ldots, v_{pi}, v_{p(i+1)}, \ldots, v_{pN}\} \quad (3)$$

The optimal value of k_i is derived using the bisection method from the corresponding calibration curve.

Parallelly, the thickness of the piezoelectric layer is evaluated by solving Equation (1) concerning d, where v_{pi} and f_r are given.

The height of the metal comes directly from the definition of k_i (Equation (4)):

$$h_i = k_i \; x \; d_i \quad (4)$$

2.4. Random Perturbator

Including fabrication tolerances in the design process is a crucial step to obtaining an optimal agreement with experimental results minimizing the necessity of trimming tools. The proposed algorithm performs this analysis by returning the Probability Density Function (P.D.F.) of the resonant frequency for arbitrary values of deposition tolerances for the piezoelectric and top electrode layers.

The random perturbator performs this through the following operations.

1. For each $k_1 \in$ A, the thicknesses of the piezoelectric and top-electrode layers are varied according to Equation (5):
$$k_i^- = \frac{h_i + \Delta h}{d_i + \Delta d} \quad (5)$$
where Δh and Δd are aleatory variables following uniform distributions between the specified values of the fabrication tolerances.
2. The resonant frequency of each ($k_i{}^-$) is estimated by taking the value of the phase velocity from the corresponding calibration curve and using Equation (6).
$$f_{ri} = v_{pi}(d_i + \Delta d) \quad (6)$$
3. Operations 1 and 2 are repeated until the convergence of the P.D.F. occurs; in this case, the algorithm is repeated 50,000 times.
4. The P.D.F. of the resonance value is obtained.

It is emphasized that using the calibration curves drastically reduces the computational time and allows the Monte Carlo simulations to be performed in a reasonable time range. For example, considering a computer using an Intel i9-9900K processor with 64 GB of RAM, FEM simulation of a single resonator requires approximately 7 min and 1.6 GB of RAM. With the same computer, the simulation of one resonator using this approach reduces the time by 2 orders of magnitude to about 30 ms.

The P.D.F. of the resonant position, exploited through the Monte Carlo simulations, is given in about 90 s when considering 50,000 iterations. If the same study had been applied with FEM models, it would have taken 243 days.

2.5. Design and Fabrication of the Resonator

Figure 2a shows an exploded view of the resonator constituted by the silicon substrate, an aluminum nitride interlayer of 186 nm, a molybdenum bottom electrode of 220 nm, a piezoelectric aluminum nitride layer, and an Aluminum top electrode.

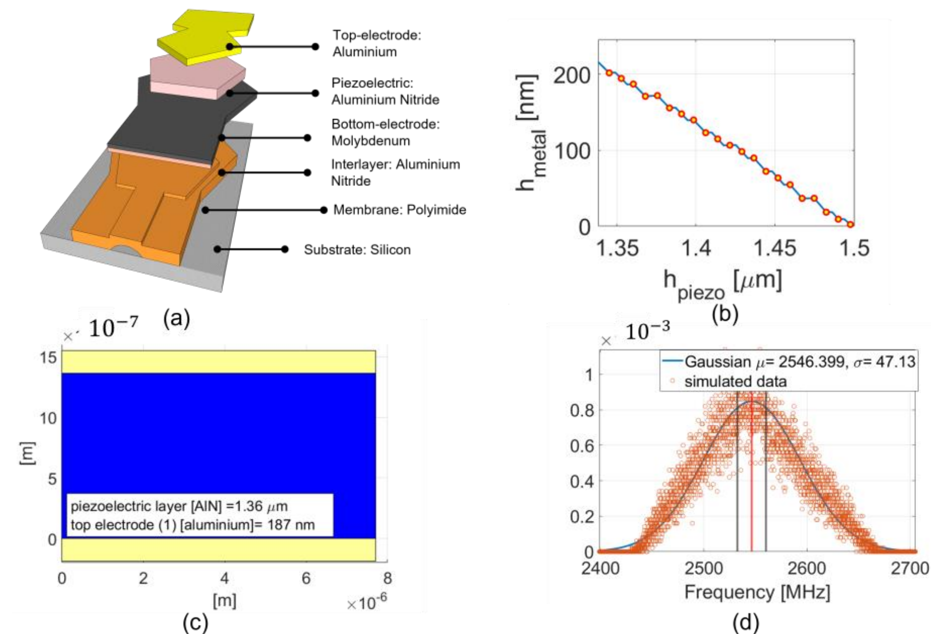

Figure 2. Resonator design using proposed innovative approach: (**a**) sketch of the resonator, (**b**) set of solutions returned by the decision algorithm, (**c**) cross-section of the selected solution, and (**d**) PDF of the resonance frequency.

Because of technological limitations, the piezoelectric thickness design requirement is restricted to a range between 1.35 µm and 1.5 µm.

Figure 2b reports all the possible solutions the decision algorithm provides. It is underlined that a total algorithm computational time of less than one minute providing 21 configurations of the resonator with piezoelectric thicknesses within the range of interest can be observed. The chosen solution is characterized by a piezoelectric thickness equal to 1.36 µm having a 187 nm thick aluminum top electrode (see Figure 2c). Because the thinner piezoelectric layer reduces the deposition times, using a thicker top electrode decreases the electrical losses, increasing the performance of the resonator.

Figure 2d shows the P.D.F. returned by the random perturbator, where layer thicknesses vary with a maximum error of 5%. The 95% confidence interval of the resonance frequency is equal to 2546 $\pm$ 23.5 MHz. In this case, the computational time is also less than one minute.

The microfabrication processing for the proposed resonator exploits an organic sacrificial layer made of Lift-Off Resist (LOR) coated with a polyimide protection layer. The role of the polymeric layer is two-fold: on one side, it prevents the dissolution of the sacrificial layer during the following steps; on the other side, the use of a flexible support layer prevents the cracking of the membrane and the collapsing of the structure.

The resonator is fabricated using four lithographic steps: the sacrificial layer, the bottom electrode, the piezoelectric layer, and the top electrode. The fabrication steps are illustrated in Figure 3.

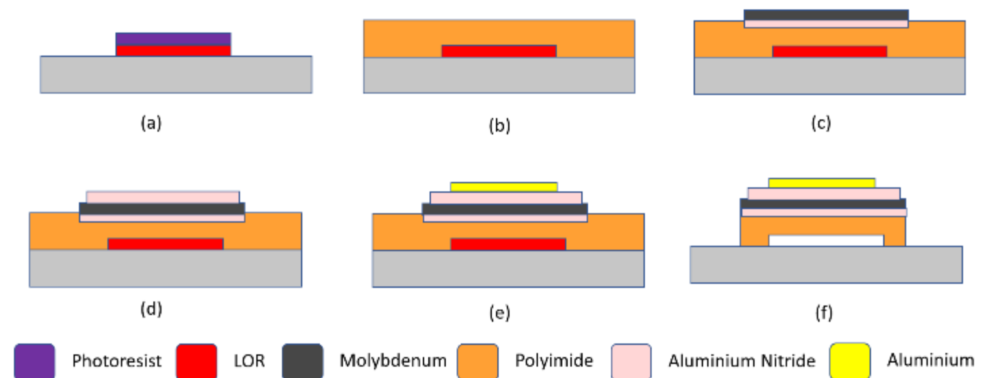

Figure 3. Fabrication protocol of the FBAR on the flexible membrane using an organic LOR sacrificial layer. (**a**) Patterning of the sacrificial layer, (**b**) covering with the protection layer, (**c**) patterning of the bottom electrode, (**d**) patterning of the piezoelectric layer, (**e**) patterning of the top-electrode, and (**f**) etching of the protection layer and releasing of the structure.

As a first step, an n-doped highly resistive silicon wafer is coated with the LOR sacrificial material. A spin-coated photosensitive resist layer on the wafer is patterned using optical lithography. During the development stage, the pattern is transferred from the photosensitive material to the sacrificial layer (Figure 3a).

After that, the resist is stripped by dipping the sample in acetone. The sacrificial layer is covered with a 2.5 µm thick polyimide protective layer (Figure 3b).

The FBAR stack form of the bottom electrode, the piezoelectric layer, and the top electrode is fabricated as described in the following paragraphs. A 186 nm thick aluminum nitride interlayer is deposited, followed by the 220 nm thick molybdenum bottom electrode. The metal and the interlayer are patterned using direct lithography and BCl3-based Inductively Coupled Plasma (ICP) etching (Figure 3c).

The piezoelectric layer is fabricated by depositing a 1.36 µm thick layer of aluminum nitride through Direct Current (DC)-pulsed sputtering and patterned with the same approach as the previous layers (Figure 3d).

The top electrode is realized with negative optical lithography, followed by the deposition of a 187 nm thick aluminum layer and a lift-off step in acetone (Figure 3e).

Finally, the polyimide protective layer is etched by an O_2-based ICP etching followed by dipping the sample in PG-Removal for 2 h to dissolve the sacrificial material (Figure 3f).

3. Results and Discussion

Figure 4 details the fabricated resonator and its characterization. Figure 4 reports an optical microscope top-view of the fabricated device. The resonator structure is analyzed through its SEM cross-section (Figure 4b), illustrating the successful release of the membrane without affecting the other materials of the stack. The measured layer thicknesses are 185 nm for the interlayer, 226 nm for the molybdenum, 1.4 µm for the aluminum nitride, and 190 nm for the aluminum. According to the Monte Carlo assumptions, these values fall within the acceptable error range (the maximum error equals 5%, while the experimental error is 3%). The device has two ports corresponding to the top and bottom electrodes. It is characterized using Vector Network Analyzer (VNA, Anritsu MS46122B, Morgan Hill, CA, USA) and Ground Signal Ground (GSG) probes (Form Factor, Z-Probe-Coaxial, Livermore, CA, USA). Figure 4c shows the modulus and the phase of the impedance of the resonator. As it can be noted, the operating frequency is equal to 2.545 GHz; indeed, it is within the confidence interval estimated by the Monte Carlo simulation in Section 3.

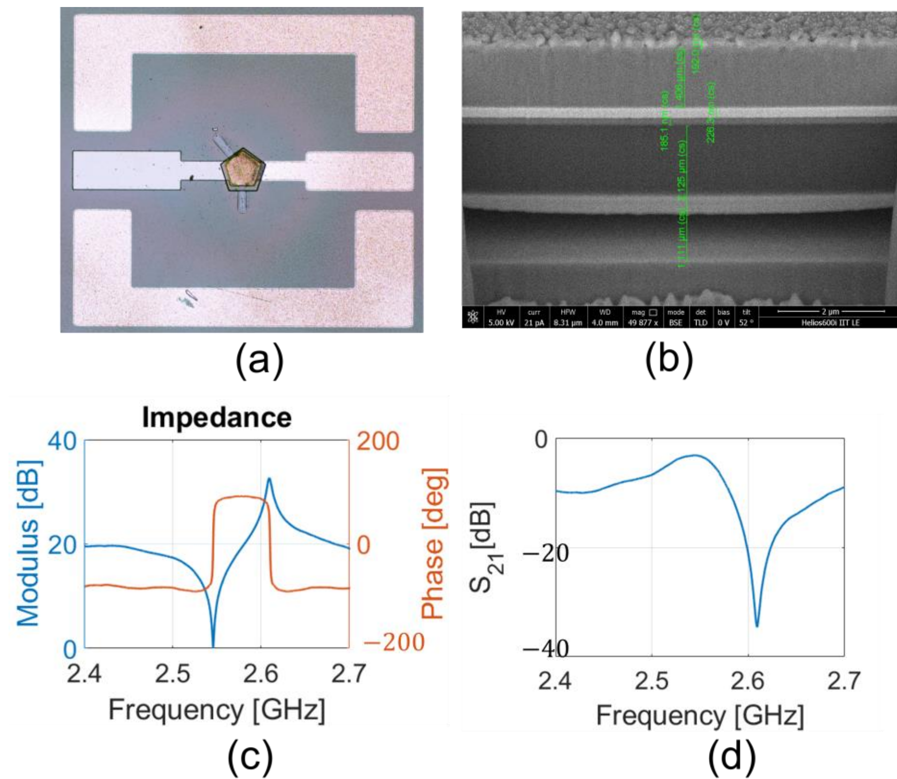

Figure 4. Characterization of the air-gap resonator. (**a**) Optical microscope top-view of the resonator, (**b**) SEM cross-section of the stack, (**c**) measured impedance of the resonator, and (**d**) scattering parameter S_{21}.

Table 1 compares the design parameters, the output of the algorithm, and the experimental results. The measurements align with the design requirements and the algorithm's forecast in terms of the obtained piezoelectric thickness and top electrode layers, considering the fabrication tolerances. The resonant frequency falls into the 95% confidence interval evaluated by the design tool with an error of 0.02% for the design requirements.

Table 1. Comparison between design requirements, the output of the algorithm, and experimental results.

	Design Requirements	The Output of the Algorithm	Experimental Results
Piezoelectric thickness (d)	1.35–1.5 µm	1.36 ± 0.07 µm	1.40 µm
Top electrode thickness (h)	-	187 ± 9.35 nm	190 nm
h/d	-	0.138	0.135
Resonant Frequency	2.550 GHz	2.550 ± 0.047 GHz	2.545 GHz

The electromechanical coupling factor and the Q-factors of the resonator are evaluated by using Equations (7) and (8):

$$k_{eff}{}^2 = (\pi/2)^2\ (f_a - f_r)/f_a \tag{7}$$

$$Q(r\,|\,a) = f/2\ \{(d\angle S_{21})/df\}\ |f = f_r\,|f_a \tag{8}$$

proving the effectiveness of the proposed fabrication protocol.

Noting that the antiresonance is at 2.601 GHz, the resonator shows optimal performance with a k^2_{eff} equal to 4.7% and Q-factors of 1426 and 1467 for the resonance and antiresonance frequencies, respectively.

Table 2 compares the design tool with the method already present in the literature. In addition, it reports a comparison of the proposed resonator to the state-of-the-art Quality factor (Q), Electromechanical coupling factor (k^2_{eff}), and Figure of Merit ($F.O.M$) parameters.

Table 2. Comparison between this work (T.W.) and the state of the art.

Ref.	Design Technique	Computational Cost	Relative Error [%]	Scalability	Fabrication Tolerances	Q	k^2_{eff}	$F.O.M.$ $Q \cdot k^2_{eff}$
[13]	FEM	HIGH	N.A.	LOW	N.A.	1548	1	1548
[14]	FEM and ECA	VERY HIGH	N.A.	LOW	N.A.	2507	2.12	5314
[15]	FEM and deep learning	HIGH	0.2–0.3	HIGH	N.A.	N.A.	N.A.	N.A.
[16]	FEM	VERY HIGH	0.2	MEDIUM	N.A.	59.8	4.1	245.18
T.W.	Calibration Curves	LOW	0.2	HIGH	Yes	1467	4.7	6895

It can be noted that with this approach, the computational costs can be drastically contained without affecting the relative error. Indeed, unlike other design processes based on FEM models, the use of calibration curves ensures faster and more lightweight simulation processes despite a contained relative error. The use of this approach makes the method highly scalable as new information can be easily added in the form of curves. In addition to the state-of-the-art, the very low computational cost allows the inclusion of fabrication tolerances exploiting Monte Carlo Simulations. Finally, thanks to the proposed fabrication protocol, the FBARs can be obtained with a very fast and straightforward process with the highest product between Q-factor and ${k_{eff}}^2$.

4. Conclusions

This paper proposes an innovative thin-film bulk acoustic wave resonator design tool powered by an upgradable library. The decision algorithm is based on exploiting the mass-loading effect. Unlike the available simulation, the only information needed is the calibration curve expressing the trend of the phase velocity versus the top-electrode thickness.

The calibration curves are reusable and arranged into a modular library that can be easily enriched with new materials, even starting from experimental data. Moreover, the algorithm includes the possibility of considering fabrication tolerances and bridging the gap between the simulations and the experimental devices.

Furthermore, the algorithm is tailored to be shared and expanded with new data refining the potential, and arbitrary values of fabrication tolerances [19].

The effectiveness of the tool is demonstrated through the design and fabrication of an innovative air-gap FBAR based on an organic sacrificial layer and with a flexible membrane. The tool is successfully taken to account for the fabrication tolerances, and the working frequency of the resonator of 2.545 GHz is within the 95% confidence interval estimated by the design tool. The proposed fabrication protocol is demonstrated to be effective and straightforward as the device has an optimal electromechanical coupling coefficient equal to 4.7% and Q-factors of 1426 and 1467 for the resonance and antiresonance frequencies, respectively. We strongly believe that this new approach represents a strategic step forward in developing high-performance FBARs and can be applied to the design and fabrication of resonators or filters.

Author Contributions: Conceptualization, G.N. and I.M., methodology, G.N., I.M., F.R. and M.G.; software, G.N.; validation, G.N. and I.M.; resources, A.D. and M.D.V.; writing—original draft preparation, G.N., I.M. and F.R.; writing—review and editing, G.N., I.M., F.R., A.D., M.G. and M.D.V.; supervision, M.G. and M.D.V. All authors have read and agreed to the published version of the manuscript.

Funding: This research received no external funding.

Institutional Review Board Statement: Not applicable.

Informed Consent Statement: Not applicable.

Data Availability Statement: Not applicable.

Conflicts of Interest: The authors declare no conflict of interest.

References

1. Ash, B.J.; Rezk, A.R.; Yeo, L.Y.; Nash, G.R. Subwavelength confinement of propagating surface acoustic waves. *Appl. Phys. Lett.* **2021**, *118*, 013502. [CrossRef]
2. Lamanna, L.; Rizzi, F.; Guido, F.; Algieri, L.; Marras, S.; Mastronardi, V.M.; Qualtieri, A.; De Vittorio, M. Flexible and Transparent Aluminum-Nitride-Based Surface-Acoustic-Wave Device on Polymeric Polyethylene Naphthalate. *Adv. Electron. Mater.* **2019**, *5*, 1900095. [CrossRef]
3. Bai, X.; Shuai, Y.; Lv, L.; Xing, Y.; Zhao, J.; Luo, W.; Wu, C.; Yang, T.; Zhang, W. The thin film bulk acoustic wave resonator based on single-crystalline 43○Y-cut lithium niobate thin films. *AIP Adv.* **2020**, *10*, 075002. [CrossRef]
4. Hara, M.; Kuypers, J.H.; Abe, T.; Esashi, M. Aluminum nitride based thin film bulk acoustic resonator using germanium sacrificial layer etching. In Proceedings of the TRANSDUCERS '03. 12th International Conference on Solid-State Sensors, Actuators and Microsystems. Digest of Technical Papers (Cat. No.03TH8664), Boston, MA, USA, 8–12 June 2003. [CrossRef]
5. Lakin, K.; Wang, J. UHF Composite Bulk Wave Resonators. In Proceedings of the 1980 Ultrasonics Symposium, Boston, MA, USA, 5–7 November 1980; pp. 834–837. [CrossRef]
6. Gao, J.; Liu, G.; Li, J.; Li, G. Recent developments of film bulk acoustic resonators. *Funct. Mater. Lett.* **2016**, *9*, 1630002. [CrossRef]
7. Ruppel, C.C.W. Acoustic Wave Filter Technology–A Review. *IEEE Trans. Ultrason. Ferroelectr. Freq. Control.* **2017**, *64*, 1390–1400. [CrossRef] [PubMed]
8. Ruby, R. 11E-2 Review and Comparison of Bulk Acoustic Wave FBAR, SMR Technology. In Proceedings of the 2006 IEEE Ultrasonics Symposium, Vancouver, DC, Canada, 3–6 October 2006; pp. 1029–1040.
9. Loebl, H.; Metzmacher, C.; Milsom, R.; Lok, P.; van Straten, F.; Tuinhout, A. RF Bulk Acoustic Wave Resonators and Filters. *J. Electroceramics* **2004**, *12*, 109–118. [CrossRef]
10. Ruby, R.; Bradley, P.; Clark, D.; Feld, D.; Jamneala, T.; Wang, K. Acoustic FBAR for filters, duplexers and front end modules. In Proceedings of the 2004 IEEE MTT-S International Microwave Symposium Digest (IEEE Cat. No.04CH37535), Fort Worth, TX, USA, 6–11 June 2004. [CrossRef]
11. Chen, Y.-C. Modeling of Thin Film Bulk Acoustic Wave Resonators and Ladder-Type Filter Design. In *Piezoelectricity, Acoustic Waves and Device Applications*; Zhejiang University: Hangzhou, China, 2007. [CrossRef]
12. Thalhammer, R.K.; Larson, J.D. Finite-Element Analysis of Bulk-Acoustic-Wave Devices: A Review of Model Setup and Applications. *IEEE Trans. Ultrason. Ferroelectr. Freq. Control.* **2016**, *63*, 1624–1635. [CrossRef] [PubMed]
13. Ashraf, N.; Mesbah, Y.; Emad, A.; Mostafa, H. Enabling the 5G: Modelling and Design of High Q Film Bulk Acoustic Wave Resonator (FBAR) for High Frequency Applications. In Proceedings of the 2020 IEEE International Symposium on Circuits and Systems (ISCAS), Seville, Spain, 12–14 October 2020; pp. 1–4. [CrossRef]
14. Pillai, G.; Zope, A.A.; Tsai, J.M.-L.; Li, S.-S. Design and Optimization of SHF Composite FBAR Resonators. *IEEE Trans. Ultrason. Ferroelectr. Freq. Control.* **2017**, *64*, 1864–1873. [CrossRef] [PubMed]
15. Morales, R.V.; Cisneros, S.O.; Perez, J.C.; Ibarra, F.S.; Carrillo, R.C. 3D Simulation-Based Acoustic Wave Resonator Analysis and Validation Using Novel Finite Element Method Software. *Sensors* **2021**, *21*, 2715. [CrossRef] [PubMed]
16. An, J.-L.; Liu, T.-T.; Gao, Y. FBAR Filter Structural Parameters Optimizing with Deep-Learning Approach. In Proceedings of the 2020 15th Symposium on Piezoelectrcity, Acoustic Waves and Device Applications (SPAWDA), Zhengzhou, China, 16–19 April 2021; pp. 428–432. [CrossRef]
17. Fu, Y.; Luo, J.; Nguyen, N.; Walton, A.; Flewitt, A.; Zu, X.; Li, Y.; McHale, G.; Matthews, A.; Iborra, E.; et al. Advances in piezoelectric thin films for acoustic biosensors, acoustofluidics and lab-on-chip applications. *Prog. Mater. Sci.* **2017**, *89*, 31–91. [CrossRef]
18. Kang, Y.-R.; Kang, S.-C.; Paek, K.-K.; Kim, Y.-K.; Kim, S.-W.; Ju, B.-K. Air-gap type film bulk acoustic resonator using flexible thin substrate. *Sens. Actuators A Phys.* **2005**, *117*, 62–70. [CrossRef]
19. Niro, G.; Marasco, I. FBARs Design Tool. 2022. Available online: https://github.com/nirogiovanni/fbar_design_tool (accessed on 10 November 2022).

Disclaimer/Publisher's Note: The statements, opinions and data contained in all publications are solely those of the individual author(s) and contributor(s) and not of MDPI and/or the editor(s). MDPI and/or the editor(s) disclaim responsibility for any injury to people or property resulting from any ideas, methods, instructions or products referred to in the content.